2020 Fifteenth International Conference on Ecological Vehicles and Renewable Energies (EVER)

Load Compensation by DSTATCOM with *LCL*-Filter by Comparing Different Resonance Damping Methods

Emre Kantar
Department of Electric Power Technology
SINTEF Energy Research
Trondheim, Norway

Elisabetta Tedeschi
Department of Electric Power Engineering
Norwegian University of Science and Technology
Trondheim, Norway

***Abstract*—This paper presents the design of a Distribution Static Compensator (DSTATCOM), interfacing the grid with an inductor-capacitor-inductor (*LCL*) filter, controlled by using $dq0$ current controller and sinusoidal pulse-width modulation (SPWM). A four-wire two-level voltage source converter (VSC) to operate as the DSTATCOM was connected at the point of common coupling (PCC) via the *LCL*-filter for neutral current compensation/load balancing, reactive power compensation, and harmonics elimination. The design of the *LCL*-filter for high switching ripple attenuation was introduced by incorporating two resonance damping techniques, namely, active damping (AD) and passive damping (PD). Besides, the design of the $dq0$ current controller was presented in detail. Load balancing, harmonic elimination, and reactive power compensation were performed using a simulation model of the DSTATCOM system. The $dq0$ current controller was implemented in the synchronous reference frame (SRF) rotating at the fundamental frequency and was composed of harmonic compensation (HC) regulators—realized by the sum of sinusoidal signal integrators (SSI)—connected in parallel to the proportional-integral (PI) regulators. Neutral current compensation was also carried out to address unbalanced loads using a 0-axis controller. Lastly, the effects of the AD and PD methods on the efficiency and dynamic performance of the system were provided.**

***Keywords*—Active power filter; DSTATCOM; harmonic elimination; *LCL*-filter; load balancing; reactive power compensation; neutral current compensation; SRF.**

I. Introduction

A large number of single-phase linear and nonlinear loads are supplied from three-phase ac mains with a neutral conductor. This, in turn, causes excessive neutral current and unbalance, and is often accompanied by high harmonics and reactive power circulations [1], [2]. While unbalance and currents in the neutral wire are a direct consequence of the single-phase uneven loads in three-phase systems, harmonics and reactive power will be there only if loads are nonlinear and have reactive components, respectively. A four-wire Distribution Static Compensator (DSTATCOM) is a shunt-connected device used for neutral current compensation/load balancing along with reactive power compensation and harmonics elimination to achieve balanced and sinusoidal source currents with Unity Power Factor (UPF) operation at the point of common coupling (PCC). Most DSTATCOMs employ a voltage source converter (VSC) supported by a dc-bus and an interface filter. A VSC can be controlled by various pulse-width-modulation (PWM) techniques to inject the desired filter currents into the PCC as a function of harmonic and reactive components of load demand along with source neutral current compensation in the event of load unbalance [3].

Conventionally, VSCs are connected to the grid using single reactors, i.e., *L*-filters [4]–[10]. However, undesired PWM switching ripples propagate to the grid due to the low attenuation ratio of *L*-filters ($20\,\mathrm{dB/dec}$). On the other hand, inductor-capacitor-inductor (*LCL*)-filters provide superior switching ripple attenuation ratio ($60\,\mathrm{dB/dec}$) by employing a smaller value of overall inductors, leading to less voltage drop and power loss [5], [9], [10]. Nevertheless, one major concern with the *LCL*-filter is the amplification of the oscillating currents at the resonant frequency (large magnitude gain caused by the *LC*). Thus, the proper design of *LCL*-filter components is of paramount importance for achieving sufficient damping at the resonant frequency to ensure the stable operation of the DSTATCOM.

The DSTATCOM control consists of two stages, that are: (i) reference filter current generation; (ii) current control scheme for switching. There are various control techniques reported for deriving the reference control signals for the DSTATCOM. Reference filter currents can be generated based on the control models of the instantaneous symmetrical component (ISC), synchronous reference frame (SRF), and instantaneous reactive power theory (IRPT) [1], [2], [11]–[13]. The reference currents are composed of fundamental and harmonic components; hence, proper current controllers are required to precisely track the components of the reference currents. An array of generalized integrators (GIs)—one for fundamental and one for each harmonic component in the stationary frame—are used in the current controllers for shunt active power filters [14]. Zero steady-state error with selective compensation is possible to attain using GIs as they can provide infinite open-loop gain and high selectivity [14], [15]. The implementation of the SRF control scheme using selective harmonic compensation (HC) of nonlinear loads was investigated in [16], [17]. For HC, sinusoidal signal integrator (SSI) regulators are used to provide sufficient compensation of harmonic load currents, where each SSI regulator can compensate for two specified harmonics in the stationary frame [17]. However, the increased number of SSIs entails heavy computational work. Since most loads are unbalanced (single-phase) and nonlinear with a nonzero neutral current, the neutral current needs to be compensated for to obtain balanced sinusoidal source currents [18].

Different topologies, reported in the literature for the DSTATCOMs, have incorporated four-leg VSCs, three single-phase VSCs, and three-leg VSCs with split capacitors, three-leg VSCs with zig-zag transformers [11], [19]. These topologies have been investigated using single reactor filters or different transformer topologies for the grid connection [20]. Three-phase four-wire DSTATCOMs have attracted much attention and are still under research [11]. However, the combination of three-phase four-wire DSTATCOMs with *LCL*-filters has not been studied extensively. In this paper, the design and control of a three-phase, four-wire, two-level VSC to operate as a DSTATCOM with an *LCL*-filter was studied. Particular emphasis was placed on investigating the advantages of an *LCL*-filter when it was combined with a DSTATCOM. The performance of the DSTATCOM was tested regarding neutral current compensation/load balancing, reactive power compensation, and harmonics elimination. Based on the SRF method, a control approach that can operate with nonlinear, unbalanced loads was implemented.

The current controller in this study generated $dq0$ reference frame signals using proportional-integral (PI) controllers with harmonic compensation–HC regulators. Due to the non-sinusoidal reference filter currents, HC regulators (tuned to particular harmonic frequency) were used to minimize the steady-state error between the reference and actual filter currents. Also, due to the nonzero neutral current caused by unbalanced loads, a 0-axis controller was required to compensate for the neutral load current. Besides, dq controllers were fed with cross-coupling and feedforward components to obtain decoupled controllers for fast dynamic response. Load balancing, harmonic elimination, and reactive power compensation were performed using a through simulation model of the DSTATCOM system, and the results were presented in detail.

For the filter design, the *LCL*-filter design methods proposed in [10] were adopted. Also, two different resonance damping methods, namely passive damping (PD) and active damping (AD), were studied. The design of the *LCL*-filter was carried out with the objectives of achieving high switching ripple attenuation ratio and setting the resonant frequency far away from the switching frequency of the DSTATCOM.

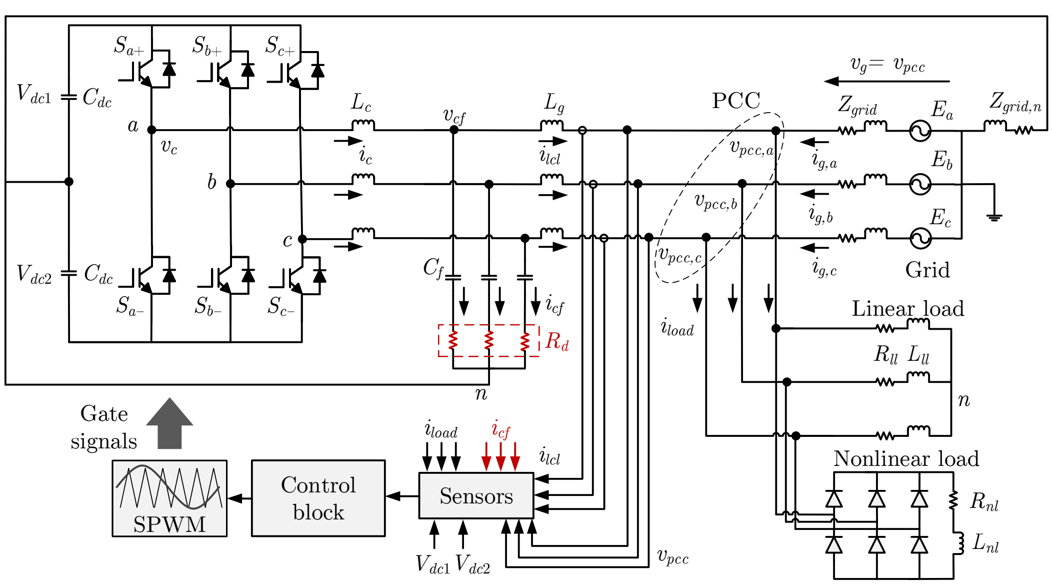

Fig. 1: Three-phase four-wire DSTATCOM with *LCL*-filter grid interface and the load connected at the PCC. The resistors R_d are used in the case of passive damping, while the currents i_{cf} are measured only in the case of active damping.

II. System Modeling

Fig. 1 presents a three-phase, four-wire, two-level DSTATCOM connected to the grid via converter- and grid-side inductors, L_c and L_g, respectively, and a filter capacitance C_f. The internal resistances are not shown in the figure explicitly. v_{pcc} stands for the phase voltages at the PCC, and i_c and i_{lcl} are the converter-side and grid-side filtered currents injected by the DSTATCOM, respectively. i_{load} represents the total load current, whereas i_g is the current injected from the source/grid. As a remark, the indices of a, b, c represent the variables in each phase, respectively. In this paper, the grid-side current feedback method (GCF)—studied in detail in [6], [10]—was adopted using i_{lcl} to close the feedback loop, as illustrated in Fig. 1. Alternatively, the converter-side-current, i_c, feedback method (CCF) could have been used with some modifications in the control loop [6], [10].

A. Overview of LCL-Filter Resonance Damping Methods

Two types of harmonics, namely, resonant harmonics, caused by the insufficient damping of the resonant poles of the system, and switching harmonics, caused by the PWM signals, exist around the resonant frequency [7], [10]. Also, switching harmonic components near the resonant frequency are amplified by the high gain magnitude at the resonance peak, leading to large oscillations [see Figs. 2(a)–(b)]. That is to say, switching harmonics also become resonance harmonics in the case of insufficient resonance damping. By neglecting the equivalent series resistances (ESRs) of filter components, the undamped gain function $G_p(s)$ of the *LCL*-filter plant is derived with reference to Fig. 3 as follows (by either ignoring the AD block, i.e., $K_d = 0$ or setting $R_d = 0$):

$$\begin{aligned}\frac{I_{lcl}(s)}{I_e(s)} &= G_c(s) \cdot G_p(s) \\ &= K_p\left(1 + \frac{1}{sT_i}\right) \cdot \frac{1}{s^3 C_f L_c L_g + s(L_c + L_g)},\end{aligned} \tag{1}$$

where $G_c(s)$ is the gain of the PI-controller where K_p and T_i represent proportional gain constant and integrator time constant, respectively. However, a nonzero s^2-term is needed in the denominator of (1) to stabilize the filter by blunting the resonance peak properly because the current controller does not contribute to the resonance damping when the GCF is utilized [10]. Internal losses caused by ESRs of the passive elements do not provide adequate damping, as depicted in Fig. 2(a), and the dynamic performance of underdamped systems is somewhat poor with very low control bandwidth [4], [5], [8]. Consequently, active or passive damping methods must be implemented to damp the resonant peak when the GCF is used [4]–[7], [21]–[24].

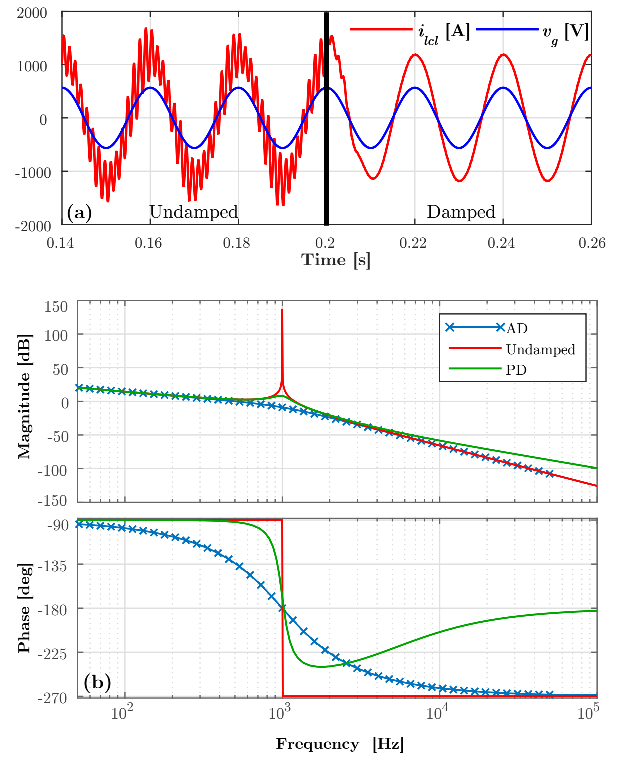

Fig. 2: (a) Open-loop magnitude and phase response of an *LCL*-filter in the cases of undamped, AD, and PD. (b) Injected grid-side current in the cases of undamped and critically damped resonance.

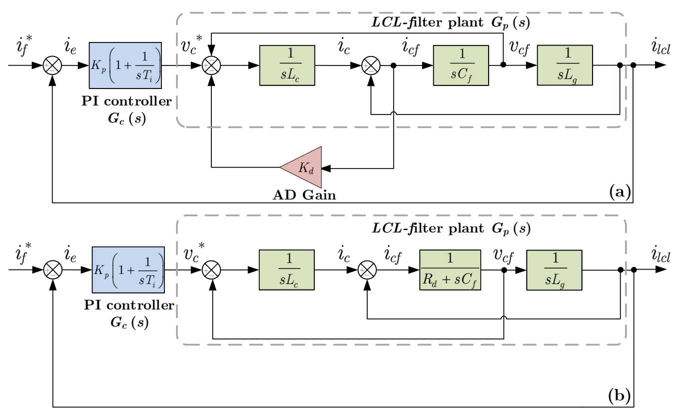

Fig. 3: Control block diagram of: (a) GCF method with AD control. (b) GCF method with PD control. i_f^*: Reference filter current, i_e: Tracking error.

The AD method modifies the reference voltage signal (v_c^*) using a virtual damping term with no loss [4]–[6], [8]. However, the design of controllers and *LCL*-filter parameters to achieve a critically damped system becomes rather complex, especially when the switching/carrier frequency has to be low such as in the case of low/medium-voltage multimegawatt converters in wind power applications [9], [25]. Besides, additional sensors to measure currents and voltages bring an extra cost.

In the literature, several AD techniques utilizing the current/voltage information through the sensors attached to the filter capacitor, converter-side inductor, or grid-side inductor have been widely applied. On the other hand, PD techniques provide a simple solution to the resonance phenomenon where resistors are inserted to the filter capacitor branch in several different ways to suppress the resonance that enables to omit sensors in this branch [4], [6], [26]. Due to the existence of nonzero impedance, change of resonant frequency owing to the aging of the components, stray inductance/capacitance in the system, or large tolerance in the components does not affect the stability of the system severely [4]. Despite these advantages in PD, towards higher frequencies in the frequency band, the third-order attenuation characteristic of the *LCL*-filter is compromised, as can also be seen in Fig. 2(b) [4], [5], [21]. Moreover, the extra losses caused by damping resistors lead to undesirable temperature rise and reduced longevity of filter elements and lower efficiency. Both strategies will be studied in detail in the following sections.

1) Active Damping Technique: In this work, the filter capacitor current, i_{cf}, was processed to achieve AD in the current control loop, as demonstrated in Fig. 3. To elaborate, in Fig. 3(a), the open-loop system consisting of an *LCL*-filter plant $G_p(s)$ and a PI controller $G_c(s)$ is fed back with the grid-side current, i_{lcl}. As can be seen in the block diagram in Fig. 3(a), the reference converter voltage value, v_c^*, is modified by a proportional P-controller with gain constant, K_d, and the resulting open-loop gain under the GCF method is derived as follows:

$$\begin{aligned}\frac{I_{lcl}(s)}{I_e(s)} &= G_c(s) \cdot G_p(s), \\ &= \frac{K_p(1+1/sT_i)}{s^3 C_f L_c L_g + s^2 K_d C_f L_g + s(L_c+L_g)}.\end{aligned} \tag{2}$$

The s^2-term in the denominator in (2) is generated by the AD gain block—which is missing in the undamped transfer function (TF) of $G_p(s)$ in (1)—and it provides the damping term, whereas the actual filter is not modified physically.

It is evident in Fig. 3(a) that the AD block functions as a notch filter, providing a negative peak response counteracting the undamped *LCL*-filter resonance [10]. This negative peak at the resonant frequency damps out the resonant peak as a function of the selected gain constant, K_d. The degree of the damping introduced in the current loop is also a function of the size of the filter components. Thus, to achieve the optimal damping factor of $\zeta = 0.707$ [6], the impedance of the filter components and the controller parameters can be fine-tuned by dividing the second-highest term to the highest term in the denominator of (2) as follows:

$$\frac{K_d}{L_c} = 2\zeta\omega_{res} = 2\zeta\sqrt{\frac{L_c+L_g}{L_c L_g C_f}}, \tag{3}$$

where ω_{res} [rad/s] is the resonant frequency of the *LCL*-filter determined solely by the passive component values.

2) Passive Damping Technique: Passive resistors are connected to the filter in various ways [4], [7], [22], [23], [27]. Cutting down on the damping losses is vital when opting for the most appropriate PD configuration [6]. Damping resistors connected in series deliver the least passive damping losses [7], while causing the highest degradation in the attenuation [4], [5]. In this work, for the PD configuration, resistors connected to the filter capacitor branch in series were used (see Fig. 1). Following the same methodology adopted for the AD method, the TF of the filter $G_p(s)$ for the PD technique under the GCF operation is derived as:

$$G_p(s) = \frac{sC_f R_d + 1}{s^3 C_f L_c L_g + s^2 C_f R_d (L_c+L_g) + s(L_c+L_g)}. \tag{4}$$

The damping factor, ζ, can be reduced from its optimal value, 0.707, to 0.5 to minimize the damping losses at the expense of compromised damping performance [6]. Similar to the AD case, R_d values to achieve the desired damping factor can be calculated by dividing the constant terms of the second-highest variable (s^2) to those of the highest variable in the denominator (s^3).

B. Reference Current Generation Using Synchronous Rotating Reference Frame

As presented in the introduction, various control algorithms can be used for the generation of reference filter currents. In this work, the control method of synchronous reference frame, SRF ($dq0$ reference frame) was used for the reference filter current generation. Current controllers employed in the SRF rotates at the fundamental frequency. For balanced and sinusoidal source currents with UPF at the PCC, the source must supply only the fundamental real component of the load current [18]. Therefore, harmonics, the reactive component of the load current, and the 0-sequence component of the load in the event of an unbalanced load should be provided by the DSTATCOM. To that end, the actual load currents are measured using sensors (in the simulations) and are transformed into the $dq0$ reference frame, as demonstrated in Fig. 4. The PCC voltages are passed to a phase-locked loop (PLL), which extracts the phase voltage magnitude and the phase angle, θ.

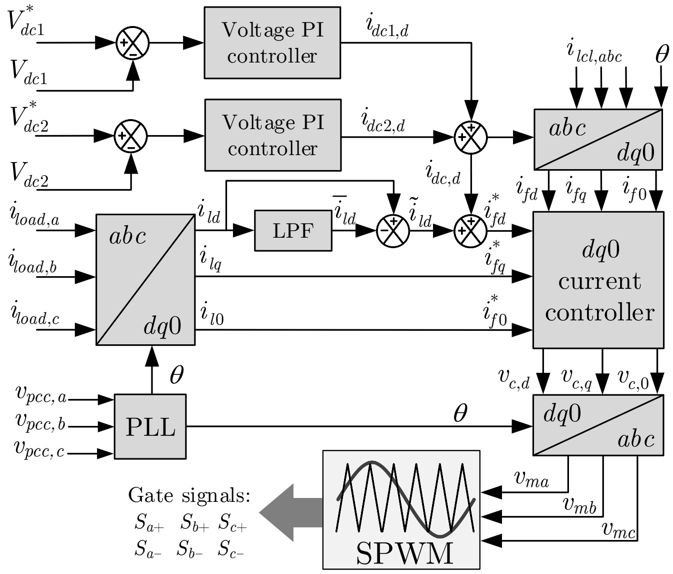

Fig. 4: Block diagram of reference signal generation for the filter current and converter voltage. GCF is implemented using $i_{lcl,abc}$.

Given the sinusoidal part of phase-a grid voltage denoted as $\cos\theta$, and hence $\theta = \omega t$, $dq0$ components rotate at the grid (line) frequency when the actual load currents are transformed into $dq0$ reference frame. Hence, the line frequency components (real part) of the load currents are dc signals, and the harmonic components become ac signals, superimposed on the dc signals as oscillations/ripples. A low-pass filter (LPF) of Butterworth type, with a cut-off frequency sufficient to allow only the dc component, is used to extract the fundamental load component, $\overline{i_{ld}}$. Then, it is subtracted from the load d-component, i_{ld} to acquire the harmonic/oscillating load component, $\widetilde{i_{ld}}$ [28]. Since the dc-link capacitors of the DSTATCOM play no role in the reactive power generation but in covering the internal losses of the switches and passive elements, the $i_{dc,d}$ component for the dc-bus voltage regulation is also added to $\widetilde{i_{ld}}$ to acquire the whole d-axis reference current. Since the entire q- and 0-axis load currents, i_{lq}, i_{l0}, are delivered by the DSTATCOM, LPFs are not needed for the q- and 0-axis components of the load, as presented in Fig. 4. The actual filter currents are processed using $i_{lcl,dq0}$ (GCF method) while the $dq0$ reference filter currents become as shown below, respectively:

$$i^*_{fd} = \widetilde{i_{ld}} + i_{dc,d}, \qquad i^*_{fq} = i_{lq}, \qquad i^*_{f0} = i_{l0}. \tag{5}$$

1) Split DC-bus Controller: As shown in Fig. 4, midpoint stabilization was performed using two identical split dc-bus PI controllers to maintain the equilibrium between V_{dc1} and V_{dc2} (in the case of the nonzero neutral current injected to the midpoint of the split dc-bus, as presented in Fig. 1).

2) Modulation Scheme: Sinusoidal PWM (SPWM) switching control was used for the generation of switching signals, as illustrated in Fig. 4. The generated voltage signals $v_{c,d}$, $v_{c,q}$, $v_{c,d}$ rotate at the speed of ω in $dq0$-frame and are transformed to the stationary-abc frame to acquire the modulation signals v_{ma} and v_{mb}, v_{mc}, which are compared with the reference triangular carrier signal [29], [30]. In the next section, using the control models introduced in this work, the design and simulation of a DSTATCOM and *LCL*-filter will be provided.

3) Current Controller with PI with HC Regulators: As DSTATCOMs are used for the compensation of unbalanced nonlinear loads, the current controllers have to address non-sinusoidal reference filter currents. When the reference current is an ac (oscillating) signal, generalized PI-controllers will cause a nonzero steady-state error due to their limited low-frequency gains [5]. However, if the reference current is a dc signal, zero steady-state error can be succeeded using a PI-controller. As mentioned in the introduction, HC is implemented using SSIs to compensate for harmonic load currents in shunt active power filter applications. SSI regulators are tuned to a particular frequency and achieve effective tracking of reference filter currents even in the case of substantial dynamic variations, and hence, improve the load compensation. In this study, HC-regulators were coupled with PI-controllers. In general, the harmonic spectrum of unbalanced, nonlinear loads incorporates current harmonics with the order of $6n \pm 1$ $(n = 1, 2, 3, ...)$ of the fundamental frequency (ω) in the stationary frame [18], [28]. Thus, one SSI regulator tuned at an integer multiple of 6ω in the $dq0$ reference frame can compensate for two specified harmonics in the stationary frame following the order of $(5, 7)$, $(11, 13)$, ... [18]. The high gain constant of the SSI in a narrow frequency band around the tuned frequency minimizes the steady-state error between the actual signal and its reference, if not entirely eliminates it. In this study, a total of six SSI regulators were employed for harmonic compensation (three for d- and three for q-controllers), as shown in Fig. 5. Thus, the harmonics up to 19^{th} in the abc-frame were regulated: $5^{\text{th}}, 11^{\text{th}}$, and 17^{th} in negative sequence, and $7^{\text{th}}, 13^{\text{th}}$, and 19^{th} in positive sequence ($6^{\text{th}}, 12^{\text{th}}$, and 18^{th} in the $dq0$ frame). The TF of the SSI unit for the d- and q-controllers is given by:

$$G_{hc}(s) = \sum_{n=1,2,3} \frac{sK_c}{s^2 + (6n\omega)^2}, \tag{6}$$

where K_c is the gain of a generalized integrator, similar to the integral gain of a PI-controller [6].

The PI-controller parameters were determined by adopting the approach described in [5]. The dq-current

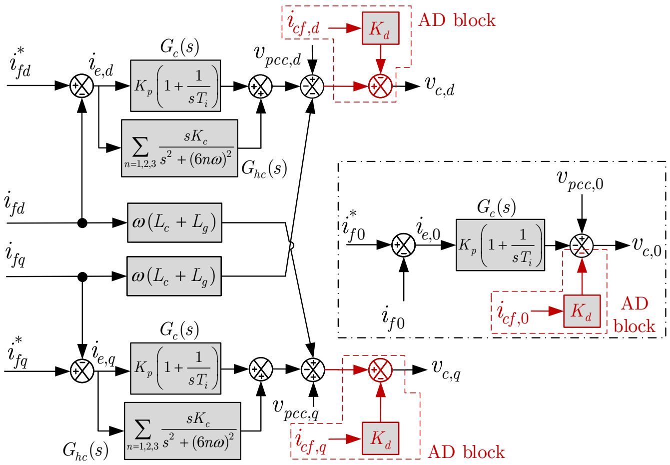

Fig. 5: Decoupled $dq0$-controllers with PI and SSI regulators. Additional control blocks for AD are presented with red boxes, which are disabled for PD.

dynamics are decoupled so that d- and q-current loops become identical and can be tuned using the same controller parameters [4]–[6], [21]. To decouple d- and q- current dynamics, the decoupling term $\omega(L_c + L_g)$ is subtracted (added) from (to) the PI controller output, and the voltage feedforward terms $v_{pcc,d}$ and $v_{pcc,q}$ are added [5], [8], as shown in Fig. 5. Also, for the AD method, the converter voltage signals are modified by using P-controllers with a gain constant K_d.

Unlike for the shunt active power filters, where the load is balanced and nonlinear with zero neutral current, the DSTATCOM current controller should also incorporate a 0-axis controller for the compensation of the neutral load current (i_{l0}) in the case of unbalanced loads [19]. In this study, a 0-axis controller was implemented in the $dq0$ reference frame using a PI-controller where i_{l0} was compared to the reference filter current i^*_{f0}.

III. Simulation Studies

The system shown in Fig. 1 was built in the simulation model. Following the proposed *LCL*-filter design algorithm proposed in [10], the filter parameters were determined. Table I shows the impedances of the source, load, feeder, filter components, and controller parameters used in the simulations. The load and feeder parameters were taken from the study performed by Geddada et al. [18]. The DSTATCOM was connected at the PCC via an *LCL*-filter for the reactive and harmonic compensation and to achieve balanced source currents under UPF operation. Both PD and AD techniques were tested.

The uncompensated terminal voltages at the PCC (before the DSTATCOM was activated) and the unbalanced nonlinear load currents are shown in Figs. 6(a) and (c), respectively. Harmonic spectrum of $i_{load,a}$ up to 50^{th} harmonic was obtained by the fast Fourier transform (FFT) [Fig. 6(d)]. To display the harmonics clearly, the

TABLE I: Simulation system parameters for the DSTATCOM.

System parameters	Simulation values
Grid voltage, frequency (V_g, f_g)	$230\,\text{V}_{rms}$, $50\,\text{Hz}$
Feeder impedance ($Z_{grid,abc}$, $Z_{grid,n}$)	$1 + j0.16\,\Omega$
Linear load, a ($Z_{ll,a}$)	$20 + j15\,\Omega$
Linear load, b ($Z_{ll,b}$)	$30 + j20\,\Omega$
Linear load, c ($Z_{ll,c}$)	$45 + j18\,\Omega$
Nonlinear load (Z_{nl})	$30 + j12\,\Omega$
DC-link voltage ($V_{dc} = 2\,V_{dc1} = 2\,V_{dc2}$)	$1100\,\text{V}$
DC-link capacitor ($C_{dc1} = C_{dc2}$)	$3.5\,\text{mF}$
LCL-parameters (L_c, L_g, C_f)	$4.5\,\text{mH}$, $4.5\,\text{mH}$, $2\,\mu\text{F}$
Current PI gains* (K_p, K_i)	50, 111000
SSI gain (K_c)	250
Voltage PI gains* (K_{pv}, K_{iv})	5, 2812
AD controller gain (K_d)	134 ($\zeta = 0.707$)
PD resistor (R_d)	$44\,\Omega$ ($\zeta = 0.707$)
PWM carrier frequency (f_c)	$10\,\text{kHz}$

* The values for the proportional and integrator gains are tuned according to symmetrical optimum [5], i.e., ($T_s = 1/fc$).

y-axis was truncated at 15% given that the fundamental component was 100%. The load current total harmonic distortion values (THD$_\text{i}$) were measured to be 11.53%, 12.52%, and 14.15% in the a, b, and c phases, respectively. After the DSTATCOM was activated at the PCC, the load compensation governed by the PI with HC current regulators in the $dq0$-frame was achieved, and the simulated PCC voltages, compensated source currents and injected filter currents at the PCC (in the case of AD) are displayed in Figs. 6(b), (e), and (g), respectively.

The PCC voltages were balanced sine curves without any switching ripple [see Fig. 6(b)]. The compensated source currents were also balanced with zero neutral currents, as shown in Fig. 6(e). UPF was achieved with a PF > 0.99 [see Fig. 6(i)], where the phase-a component had a THD$_\text{i}$ around 2.15% with a clear contribution of odd harmonics, as shown in Fig. 6(f). Besides, the injected DSTATCOM currents through the *LCL*-filter are shown in Fig. 6(g), where the DSTATCOM supplied the neutral/0-sequence load current while the source only supplied the real power demand of the load. The harmonic content of the injected phase-a current is shown in Fig. 6(h).

Fig. 6(j) depicts the phase-a currents $i_{g,a}$, $i_{c,a}$, $i_{cf,a}$, and $i_{load,a}$. It was observed that C_f absorbed the switching ripple, and hence a considerable amount of ripple (discernible on $i_{c,a}$) was cleared off of $i_{lcl,a}$. Tracking achieved by PI and HC regulators employed in the $dq0$-current control loop is demonstrated in Fig. 7. The dashed lines show the reference currents while the solid lines represent the actual filter currents. Apparently, high gain of the SSIs for tuned frequency signals improved the tracking performance and minimized the tracking error between the controlled and reference signals [28].

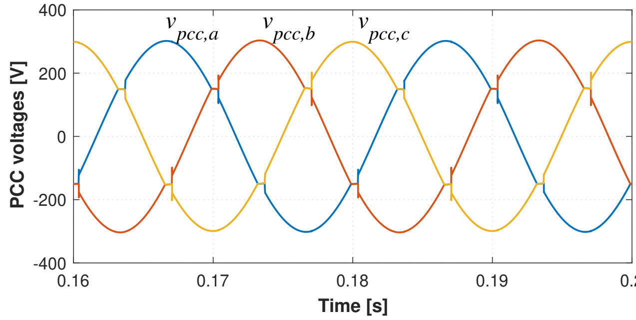

(a)PCC voltages before compensation by the DSTATCOM ($\mathrm{THD_v} = 2.97\%$).

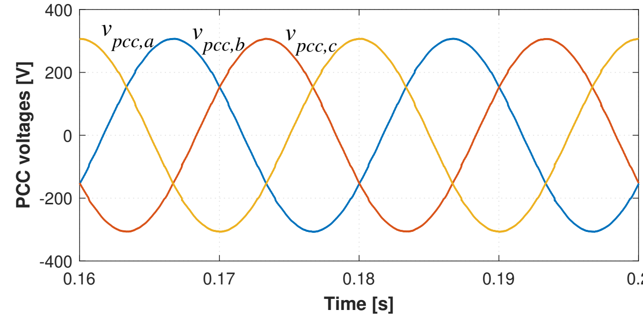

(b) PCC voltages after compensation by the DSTATCOM ($\mathrm{THD_v} = 0.44\%$).

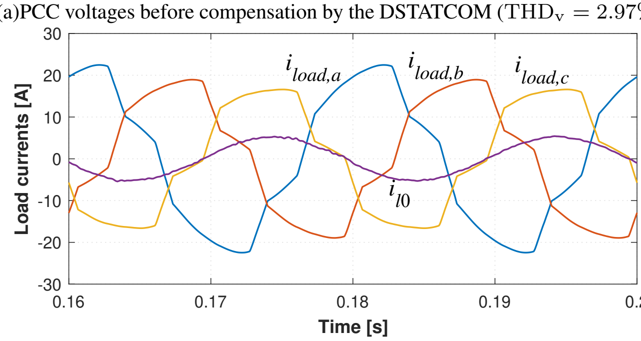

(c) Unbalanced, nonlinear load currents.

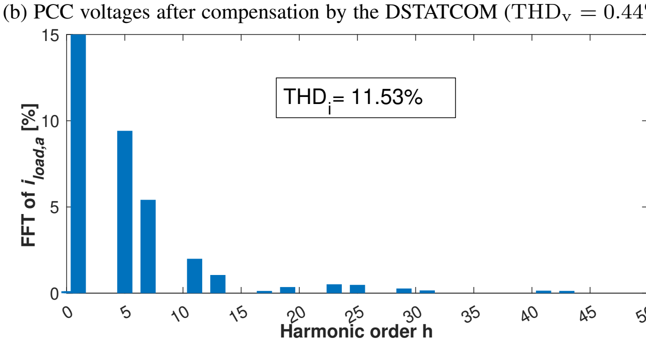

(d) Harmonic spectrum of $i_{load,a}$ extracted by FFT.

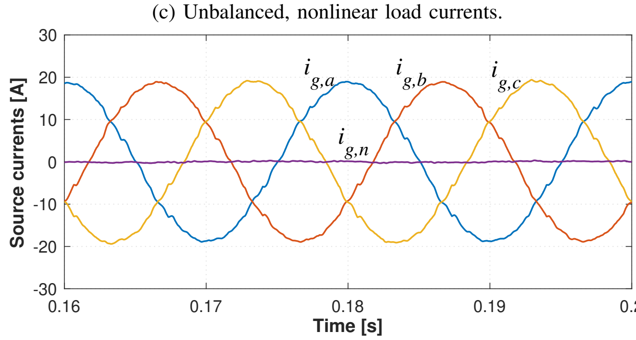

(e) Source currents supplied by the grid at the PCC after compensation.

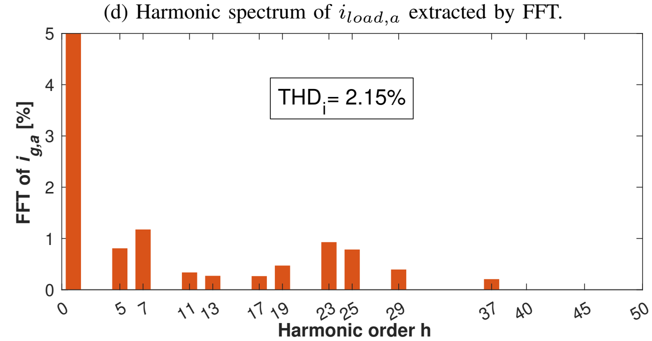

(f) Harmonic spectrum of $i_{g,a}$ extracted by FFT after compensation.

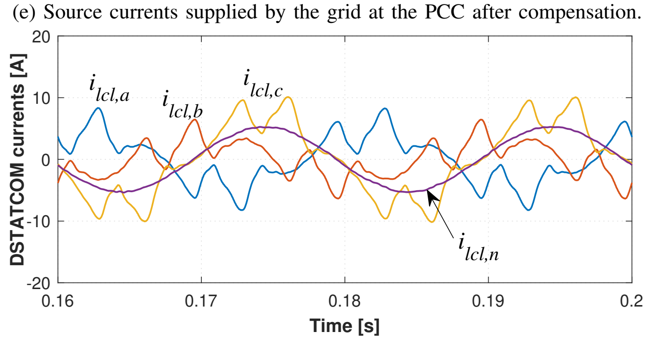

(g) Compensation currents injected by the DSTATCOM via the *LCL*-filter.

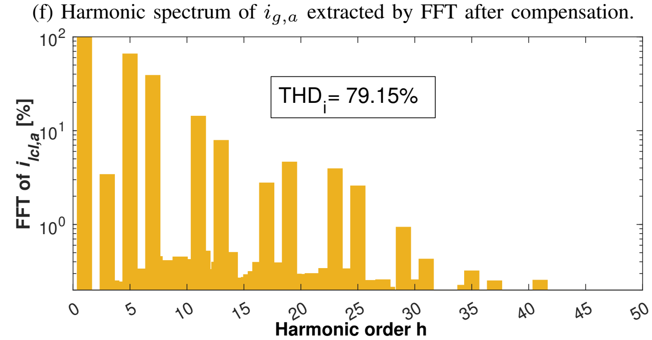

(h) Harmonic spectrum of $i_{lcl,a}$ extracted by FFT (compensation currents).

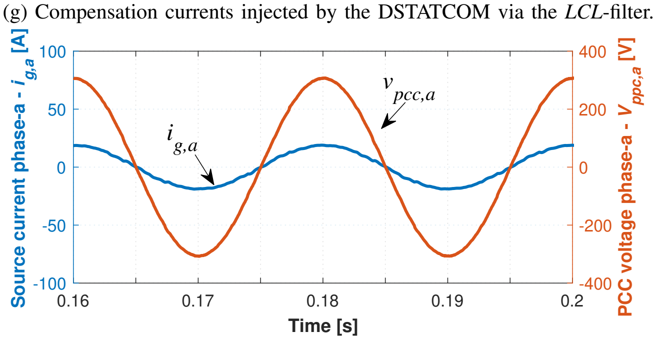

(i) Phase-a source current $v_{pcc,a}$ vs. phase-a source current $i_{lcl,a}$ (PF= 0.99).

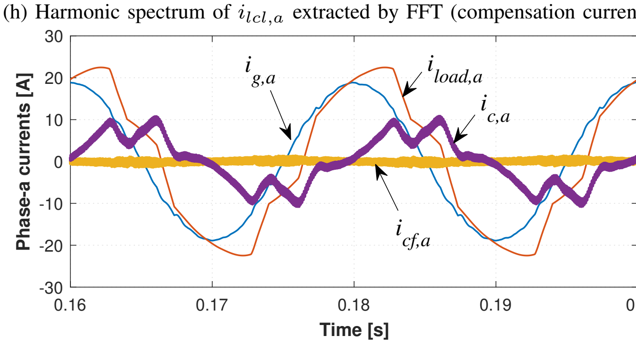

(j) Phase-a source currents: $i_{g,a}$, $i_{load,a}$, $i_{c,a}$, $i_{cf,a}$.

Fig. 6: Simulations results of the uncompensated and compensated system (in the case of AD): PCC voltages, source currents, load currents, grid-side and converter-side DSTATCOM currents, harmonic components by the FFT analyses. Results in the case of PD look identical.

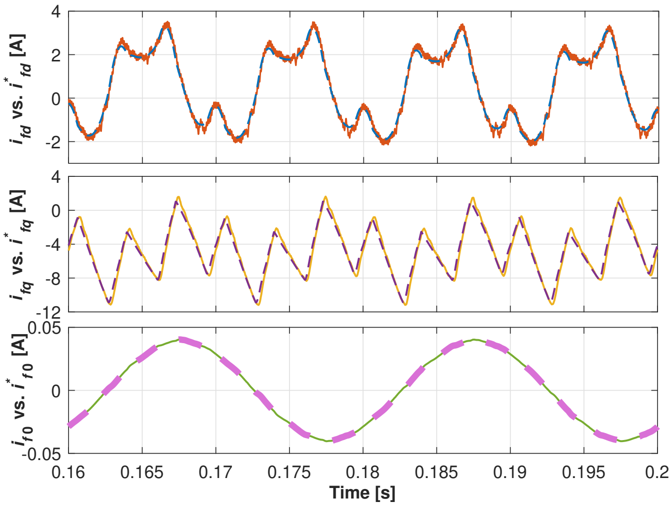

Fig. 7: Reference and actual filter currents in the $dq0$ frame. Dashed-lines represent the reference signals.

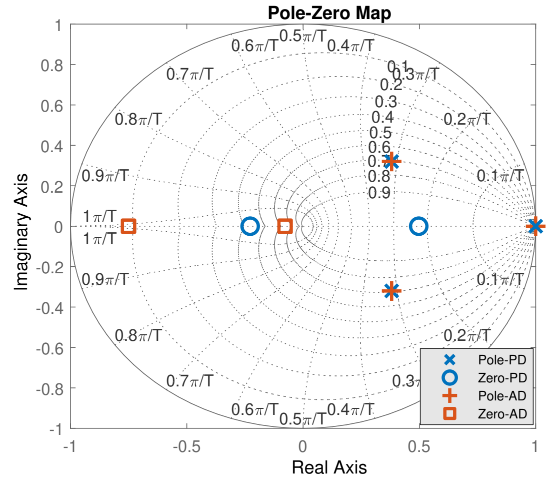

Fig. 8: Impact of different damping methods on the system pole-zero locations in the continuous s-plane (PWM unit and PI controllers are neglected).

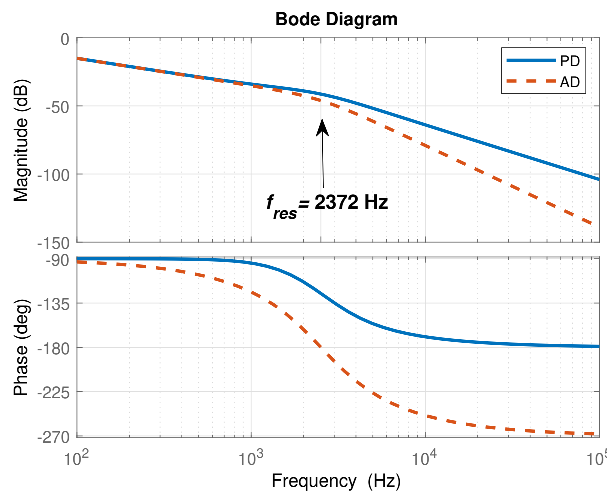

Fig. 9: Bode plot of the open-loop magnitude and phase response of an *LCL*-filter for AD and PD.

IV. Discussion

The attenuation achieved by an *L*-filter is $20\,\mathrm{dB/dec}$ over the entire frequency range as opposed to the 60-$\mathrm{dB/dec}$ attenuation provided by an *LCL*-filter. A simulation study was performed to compare the attenuation of an *LCL*-filter to an *L*-filter for the same system based on the ripple percentage in the source current and voltage. For the same ripple percentage (5%) in the source current and voltage, a significantly larger overall filter inductance of $30\,\mathrm{mH}$ (by a factor of 3.3) would be needed in the case of *L*-filter. In a similar application, Geddada et al. [18] also reported reduced overall filter inductance by a factor of 3.5 for the same ripple percentage. Else, the switching frequency would be increased for sufficient attenuation of ripples that would increase the total losses and stress the semiconductors further (use of higher-rated switches would be inevitable). Hence, the benefits provided by the *LCL* in terms of attenuation, cost, and size far outweigh the complexity in controller design. That is to say, interfacing the DSTATCOM with grid via an *LCL*-filter as an alternative for a single inductor provides significantly improved harmonic compensation, particularly by reducing the high-frequency switching harmonics caused by the PWM unit.

To address the extra complexity incurred in the controller design due to the *LCL*-filter, AD and PD methods were used. The simulation results shown in Figs. 6–7 were acquired by using the AD technique. This part of the discussion will provide performance benchmarking of the AD and PD methods. For the purpose of analysis, pole-zero maps of the open-loop filter plants with AD and PD were plotted (Fig. 8) using $G_p(s)$ in (2) and (4). The values shown in Table I were substituted into the corresponding TFs. As shown, the calculated R_d and K_d values provided the optimal damping factor, $\zeta = 0.707$.

To shed more light on the dynamic performance of the PD and AD methods, Bode plots for the *LCL*-filter plants are presented in Fig. 9 under each method. As seen, both methods led to a closed-loop stable system, whereas the AD provided higher harmonic attenuation than the PD did at frequencies higher than the resonance frequency (2372 Hz). To test the dynamic response of the control system with the AD or PD, step responses of the dc-link voltage and the control currents were performed. The dc-link voltage V_{dc1} seemed to be maintained around $550\,\mathrm{V}$ within an acceptable envelope ($\pm 0.5\,\mathrm{V}$)—see Fig. 10(a). Also, the step responses of the dc-bus voltage V_{dc1} under both methods indicated that, with the proper tuning of the controller parameters, fast response with adequate resonance damping (non-oscillatory) can be obtained using either method.

In both methods, the step responses of the actual $dq0$-currents to the load change, shown in Fig. 10(b), seemed to be fast and robust with acceptable overshoots.

Also, no high-frequency oscillations were observed at the transition from no-load to full-load, indicating that the system was damped adequately. Hypothetically speaking, if the resonance peak were underdamped, high-frequency transients would appear, as illustrated in the top figure in Fig. 10(b). It, thus, would compromise on the transient performance that might lead to oscillations likely to cause loss of stability in the controllers. Dynamic and steady-state performances of the AD and PD methods are summarized in Table II.

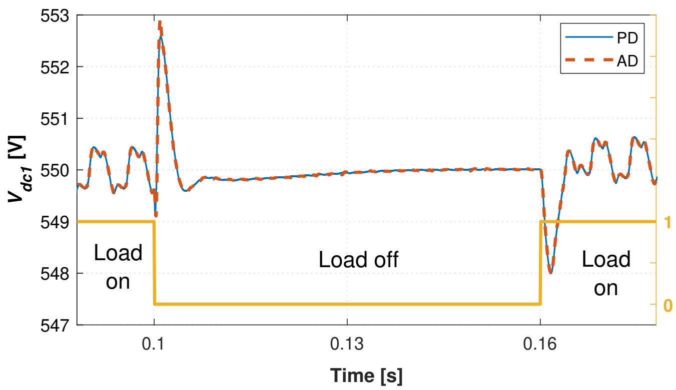

(a) Impact of the load change on the step response of the dc-bus voltage.

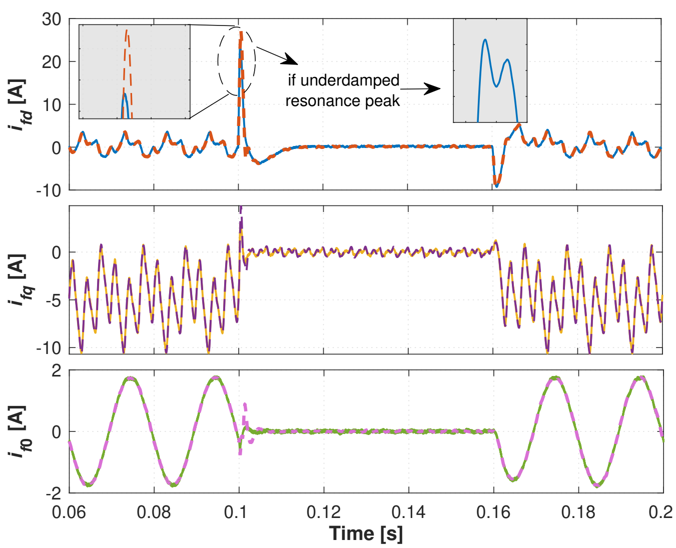

(b) Step response of $dq0$-currents to load change (off between $0.1-0.16$ s).

Fig. 10: The dynamic performance of the DSTATCOM for reactive current compensation in the UPF mode. Solid line: the PD method, dashed line: the AD method.

TABLE II: Dynamic and steady-state performances of PD and AD.

Performance	**Passive damping**	**Active damping**
Step response	Excellent	Good
Resonance damping	Adequate	Adequate
$\mathrm{THD_v}$ (%) of $v_{pcc,abc}$	1.10, 1.11, 1.11	0.43, 0.44, 0.44
$\mathrm{THD_i}$ (%) of $i_{g,abc}$	2.44, 2.48, 2.39	2.15, 2.20, 2.21
Damping loss (W)	16.6, 17.4, 17.5	0, 0, 0

THDs of the PCC voltages and the source currents in each method appeared to be significantly lower than the acceptable limits according to IEEE-519-1992 and EN50160 standards. As seen from the step responses and the THD values, there was a trade-off between transient and damping performances. That is to say, the faster step response in the case of PD was compromised by the increased high-frequency oscillations injected into the PCC voltage and currents (vice versa for the AD).

Source currents in both methods had $\mathrm{THD_i}$s up to 2.5% with a clear contribution of odd harmonics, as shown in Fig. 6(f). These odd harmonics stemmed from the nonzero tracking error, i_e, between the reference and injected filter currents, as depicted in Fig. 11. Although the errors were significantly reduced using HC regulators (SSIs) in addition to the PI regulators in the $dq0$ controller, the fine-tuning of the SSI gain constant K_c for individual odd harmonics is likely to further lessen the error. Furthermore, increasing the number of SSIs to span a larger frequency spectrum as well as fine-tuning of the PI-controller parameters may reduce the error further.

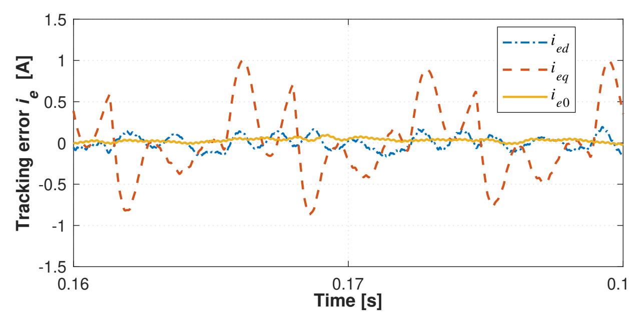

Fig. 11: Tracking error i_e: $i_{ed} = i^*_{fd} - i_{fd}$, $i_{eq} = i^*_{fq} - i_{fq}$ and $i_{e0} = i^*_{f0} - i_{f0}$.

Lastly, damping resistors, R_d, used in the case of PD, cause additional damping losses calculated by:

$$P_d = R_d \sum_h \left[i_c(h) - i_{lcl}(h)\right]^2 = R_d \sum_h \left[i_{cf}(h)\right]^2, \quad (7)$$

where P_d represents the damping loss in each phase, and h indicates harmonic components extracted from the FFT analysis [4]. The total damping loss, computed using (7), was $51.5\,\mathrm{W}$ that corresponds to 1.5% of the total apparent power of the DSTATCOM ($3.4\,\mathrm{kVA}$).

V. Conclusion

The compensation of unbalanced nonlinear loads has been carried out satisfactorily by the *LCL*-filter DSTATCOM using a $dq0$-current controller (SRF method) with SPWM switching. Neutral current compensation/load balancing, reactive power compensation, harmonic elimination of source currents with UPF were achieved, and $\mathrm{THD_i}$s were maintained at lower than 3% although the load current THDs were around 11%. AD and PD methods were shown to be effective in addressing the resonance phenomenon caused by the *LCL*-filter. Consequently, the voltage at the PCC was maintained with THDs less than 1.2% under nonlinear, unbalanced loads in both methods. Higher switching ripple attenuation at the terminal voltages and source currents were obtained in the case of the AD method with satisfactory dynamic performance and zero damping losses, whereas the PD method brought about 1.5% additional losses.

REFERENCES

[1] H. Akagi, S. Ogasawara, and Hyosung Kim, "The theory of instantaneous power in three-phase four-wire systems: a comprehensive approach," in *1999 IEEE Indust. App.*, vol. 1, Oct. 1999, pp. 431–439.

[2] H. Akagi, "Generalized theory of the instantaneous reactive power in three-phase circuits," *IEEJ IPEC-Tokyo*, 1983.

[3] T. Zaveri, B. Bhalja, and N. Zaveri, "Comparison of control strategies for DSTATCOM in three-phase, four-wire distribution system for power quality improvement under various source voltage and load conditions," *Int. J. Electr. Power Energy Sys.*, vol. 43, no. 1, pp. 582–594, 2012.

[4] M. Liserre, F. Blaabjerg, and S. Hansen, "Design and control of an LCL-filter-based three-phase active rectifier," *IEEE Trans. Ind. Appl.*, vol. 41, no. 5, pp. 1281–1291, 2005.

[5] J. Dannehl, F. W. Fuchs, S. Hansen, and P. B. Thøgersen, "Investigation of active damping approaches for PI-based current control of grid-connected pulse width modulation converters with LCL filters," *IEEE Trans. Ind. Appl.*, vol. 46, no. 4, pp. 1509–1517, 2010.

[6] Y. Tang, P. C. Loh, P. Wang, F. H. Choo, and F. Gao, "Exploring inherent damping characteristic of LCL-filters for three-phase grid-connected voltage source inverters," *IEEE Trans. Power Electr.*, vol. 27, no. 3, pp. 1433–1443, 2012.

[7] B. G. Cho and S. K. Sul, "LCL filter design for grid-connected voltage-source converters in high power systems," in *IEEE En. Conv. Cong. Expo. (ECCE)*, Sept. 2012, pp. 1548–1555.

[8] J. Dannehl, C. Wessels, and F. W. Fuchs, "Limitations of voltage-oriented PI current control of grid-connected PWM rectifiers with filters," *IEEE Trans. Ind. Electr.*, vol. 56, no. 2, pp. 380–388, 2009.

[9] A. Rockhill, M. Liserre, R. Teodorescu, and P. Rodriguez, "Grid-filter design for a multimegawatt medium-voltage voltage-source inverter," *IEEE Trans. Ind. Electr.*, vol. 58, no. 4, pp. 1205–1217, 2011.

[10] E. Kantar and A. M. Hava, "LCL-filter design for low-voltage high-power grid-tied voltage-source converter considering various damping methods," in *IEEE 17th Control Modeling Power Electr. (COMPEL)*, 2016, pp. 1–8.

[11] B. Singh, P. Jayaprakash, S. Kumar, and D. P. Kothari, "Implementation of neural-network-controlled three-leg VSC and a transformer as three-phase four-wire DSTATCOM," *IEEE Trans. Ind. App.*, vol. 47, no. 4, pp. 1892–1901, July 2011.

[12] B. Singh, P. Jayaprakash, and D. Kothari, "New control approach for capacitor supported DSTATCOM in three-phase four wire distribution system under non-ideal supply voltage conditions based on synchronous reference frame theory," *Int. J. Electr. Pow. En. Sys.*, vol. 33, no. 5, pp. 1109 – 1117, 2011.

[13] R. S. Herrera and P. Salmeron, "Instantaneous reactive power theory: A reference in the nonlinear loads compensation," *IEEE Trans. Ind. Electr.*, vol. 56, no. 6, pp. 2015–2022, June 2009.

[14] X. Yuan, W. Merk, H. Stemmler, and J. Allmeling, "Stationary-frame generalized integrators for current control of active power filters with zero steady-state error for current harmonics of concern under unbalanced and distorted operating conditions," *IEEE Trans. Ind. App.*, vol. 38, no. 2, pp. 523–532, 2002.

[15] P. Mattavelli, "A closed-loop selective harmonic compensation for active filters," *IEEE Trans. Ind. App.*, vol. 37, no. 1, pp. 81–89, 2001.

[16] C. Lascu, L. Asiminoaei, I. Boldea, and F. Blaabjerg, "High performance current controller for selective harmonic compensation in active power filters," *IEEE Trans. Pow. Electr.*, vol. 22, no. 5, pp. 1826–1835, Sept. 2007.

[17] R. I. Bojoi, G. Griva, V. Bostan, M. Guerriero, F. Farina, and F. Profumo, "Current control strategy for power conditioners using sinusoidal signal integrators in synchronous reference frame," *IEEE Trans. Pow. Electr.*, vol. 20, no. 6, pp. 1402–1412, Nov. 2005.

[18] N. Geddada, M. K. Mishra, and M. M. Kumar, "LCL filter with passive damping for DSTATCOM using PI and HC regulators in dq0 current controller for load compensation," *Sus. En. Gr. Netw.*, vol. 2, pp. 1–14, 2015.

[19] L. A. Vitoi, D. I. Brandao, and E. Tedeschi, "Power quality enhancement by SiC Active Power Filters in Oil and Gas Platforms," in *IEEE En. Conv. Cong. Expo. (ECCE)*, Sept. 2019, pp. 4299–4304.

[20] B. Singh, P. Jayaprakash, and D. P. Kothari, "A T-Connected transformer and three-leg VSC based DSTATCOM for power quality improvement," *IEEE Trans. Power Electr.*, vol. 23, no. 6, pp. 2710–2718, Nov. 2008.

[21] S. G. Parker, B. P. McGrath, and D. G. Holmes, "Regions of active damping control for LCL filters," *IEEE Trans. Ind. Appl.*, vol. 50, no. 1, pp. 424–432, 2014.

[22] S. Parker, B. McGrath, and D. Holmes, "A general discrete time model to evaluate active damping of grid converters with LCL filters," in *IEEE Proc. Int. Power Electr. Conf. (IPEC-Hiroshima-ECCE ASIA)*, 2014, pp. 2019–2026.

[23] E. Kantar, S. N. Usluer, and A. M. Hava, "Control strategies for grid connected PWM-VSI systems," in *IEEE Proc. 8th Int. Conf. Elect. Electr. Eng. (ELECO)*, Nov. 28–30, 2013, pp. 220–224.

[24] S. N. Usluer and A. M. Hava, "Investigation on series active filter compensated high power grid-connected voltage source inverters with LCL filter," in *IEEE En. Conv. Cong. Expo. (ECCE)*, Sept. 2014, pp. 381–388.

[25] E. Kantar and A. M. Hava, "Design of grid connected PWM converters considering topology and PWM methods for low-voltage renewable energy applications," in *IEEE Proc. Int. Power Electr. Conf. (IPEC-Hiroshima-ECCE ASIA)*, 2014, pp. 2034–2041.

[26] E. Kantar, S. N. Usluer, and A. M. Hava, "Design and performance analysis of a grid connected PWM-VSI system," in *IEEE Proc. 8th Int. Conf. Elect. Electr. Eng. (ELECO)*, Nov. 28–30, 2013, pp. 157–161.

[27] H. Brantsæter, Ł. Kocewiak, A. R. Årdal, and E. Tedeschi, "Passive filter design and offshore wind turbine modelling for system level harmonic studies," *Energy Procedia*, vol. 80, pp. 401 – 410, 2015.

[28] N. Geddada, S. B. Karanki, and M. K. Mishra, "DSTATCOM with LCL filter using synchronous reference frame current controller," in *Int. Conf. Clean Electr. Power (ICCEP)*, June 2013, pp. 796–802.

[29] E. Kantar, "Design and control of PWM converter with LCL type filter for grid interface of renewable energy systems," M.S. thesis, Elect. and Electr. Eng. Dept., Middle East Tech. Uni., July 2014, Ankara, Turkey.

[30] E. Kantar and A. M. Hava, "Optimal design of grid-connected voltage source converters considering cost and operating factors," *IEEE Trans. Ind. Electr.*, vol. 63, no. 9, pp. 5336–5347, 2016.